

# Smart Floating Balls: 3D Printed Spherical Antennas and Sensors for Water Quality Monitoring

Wenjing Su, Shicong Wang, Ryan Bahr, and Manos M. Tentzeris  
School of Electrical and Computer Engineering, Georgia Institute of Technology  
Email: wenjing.su.gatech@gmail.com

**Abstract**—This paper proposes a novel additively manufactured floating ball sensor for water monitoring applications. A chipless RFID phase modulation configuration is used along with spherical patch antennas and phase delay microstriplines that are sensitive to the liquid content. The spherical patch antenna array provides omni-directional gain in water level plane and can be used in MIMO applications in the water. The phase delay line utilizes a microfluidic channel embedded into the microstripline so that the phase introduced by the line can be reconfigured by the liquid inside the channel. Due to its complex shape, the floating ball fabrication process combines both 3D printing and 3D stamping, which enables selective 3D metalization using the same platform. The smart floating ball can monitor reservoir water quality while preserving its original function as a “shadow ball” featuring low-cost, light-weight and battery-less, which are important features for massively scalable “smart” systems.

**Index Terms**—wireless sensing, chipless RFID, liquid monitoring, 3D printing, additive manufacturing, smart environment

## I. INTRODUCTION

There are over 80,000 reservoirs in US, meaning that potential water contamination could have catastrophic health effects. Many reservoirs use floating “shadow balls” to save water by reducing evaporation. What if those floating balls could simultaneously monitor the reservoir water quality and give timely warning? Therefore, we propose the topologies of smart floating balls with spherical antennas on top featuring omni-directional radiation performance along the plane of water surface along with embedded liquid wireless sensors that are capable of detecting water contamination, such as oil and gas wastewater. These smart floating ball can be also used in other liquid monitoring applications, such as crude leakage in oceans.

3D printing, especially low-cost dielectric 3D printing, has been involved in the fabrication of antennas and microwave components recently[1], [2], due to its simplicity in printing light-weight complex-shape 3D objects. However, due to the challenge of selectively metalizing the dielectric 3D objects, most prior efforts have focused on structures that are fully coated with metal such as horn antennas[3] and waveguides[4]. Selective metalization methods has been proposed by few researchers, which usually require multiple steps and very expensive manufacturing tools. In this paper, we propose a straight-forward but easily scalable approach, the 3D printed conformal stamp. While low-cost dielectric 3D printing enables fabrication of complex shape 3D objects without assembly, 3D printed conformal stamp enables on-demand metalization of these complex 3D dielectric surfaces

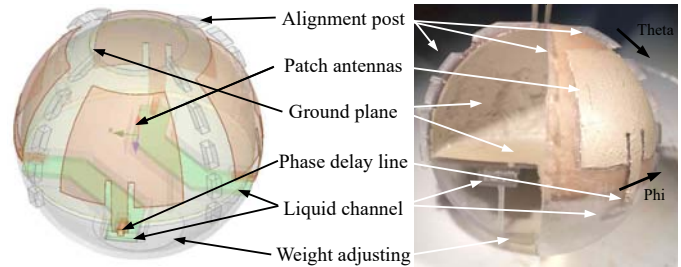


Fig. 1. A graph of the smart floating ball and a cross-section photo of a proof-of-concept prototype.

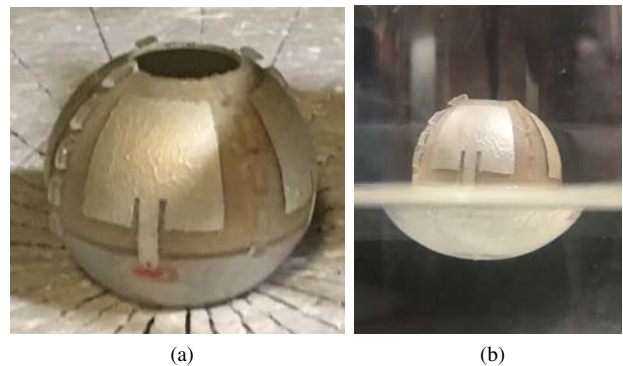


Fig. 2. Photo of fabricated prototypes of a smart floating ball based on the spherical patch antennas in (a) along with a photo showing it floating on water in (b).

enabling the easy realization of high-complexity RF modules, such as the smart floating balls. By adopting this stamping approach, a single 3D dielectric printing platform can enable fabrication of virtually any 3D microwave components/passive systems on-demand at a low cost without assembly.

## II. FABRICATION

The fabrication process contains two steps: printing dielectric structures and then selectively metalizing them. The complex dielectric structure shown in Fig. 1 would be extremely hard to fabricate with any traditional fabrication methods due to the spherical 3D shape, hollow interior and miniaturized microfluidic. However, the complexity of the structure can be easily resolved with 3D printing technique. The Form Labs clear resin was used for a proof-of-concept prototype of the dielectric structure featuring a permittivity around 2.8 and loss tangent around 0.03. The metalization was realized by using a 3D printed stamp. The Form Labs flexible resin provides a soft surface with a great wettability that would be necessary

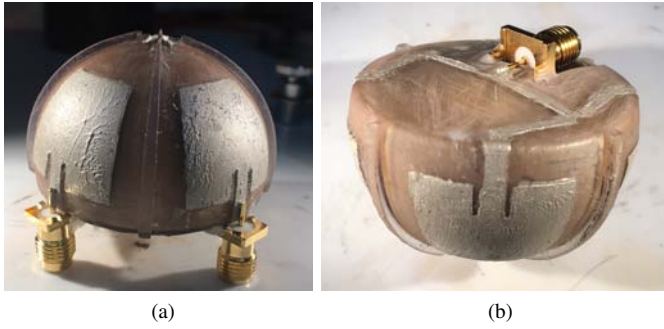


Fig. 3. Photos of fabricated prototypes of (a) four spherical patch antennas, (b) a  $4 \times 1$  patch array around the top hemisphere interconnected with a power splitter on the bottom plane, and (c) a smart floating ball based on the spherical patch antennas floating on water.

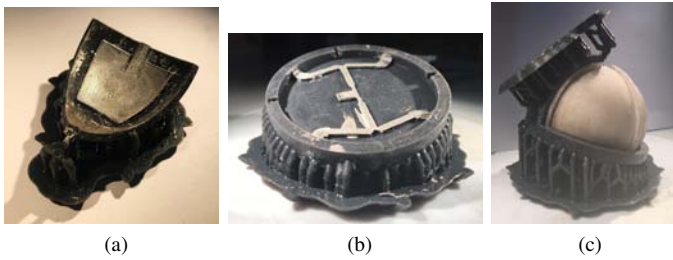


Fig. 4. 3D printed conformal stamp. Photos of (a) the stamp for the spherical patch antennas, (b) the stamp for the power splitter utilized in the antenna array in Fig. 3b, and (c) stamping both stamps for the composite antenna array topology of Fig. 3b.

for high-quality stamping. The pattern to be stamped is 1 mm higher than the unpatterned section of the stamp and 0.1 mm higher on the dielectric structure so that the pattern with ink can be easily transform from the stamp to the dielectric without touching the unpattern surface. Compared to normal stamps, this 3D printed stamp can be made conformal to any surface, including curved surfaces and corners as shown in Fig. 4, which enables metalization on any arbitrary 3D object surface.

To proof the concept and to investigate the performance of different part of the smart floating ball, a complete ball including antennas and sensors (Fig. 2), a top half ball with four individual antennas (Fig. 3a), and a top half ball with a four-antenna array (Fig. 3b), were printed and selectively metalized. Fig. 4a and Fig. 4b show the stamps for a spherical patch antenna and for a power splitter, respectively. Rectangular posts are printed on the dielectric spherical structure for proper alignment as shown in Fig. 4c. The utilized ink for the stamp is LPKF proconduct paste, however, any conductive ink can be used for stamping. The interior of the top hemisphere, which is the ground plane in this design, and the phase delay lines/sensors (Fig. 1, Fig. 2 and Fig. 9a) were metalized massively/unselectively by simply depositing and coating with the same silver paste. Then the ink was cured at  $80^{\circ}\text{C}$  for 1 hour and  $0.06 \text{ Ohm/square}$  was achieved. The fabrication of both complex shape smart floating ball and the metallization stamp is carried out by a single low-cost stereolithography (SLA) 3D printer, which can largely simplify the process and

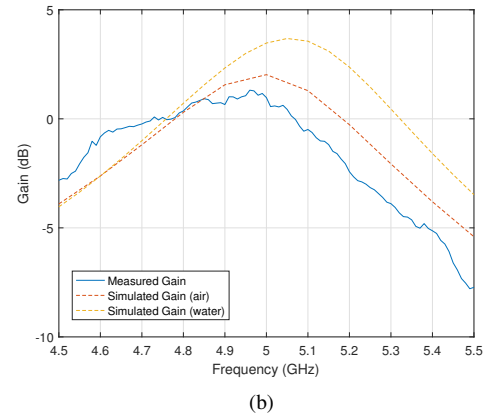
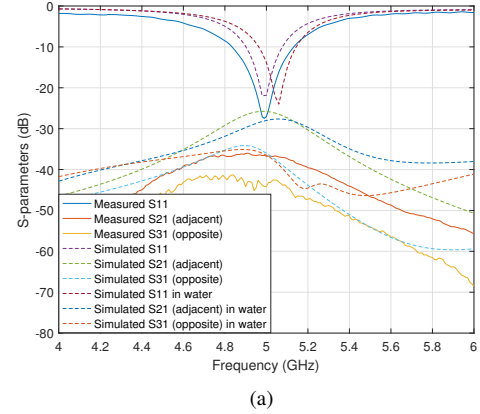


Fig. 5. Performance of the four individual antennas on the sphere. Measured and simulated values in air and simulated values in water for (a) return loss of the antenna and coupling between antennas and (b) gain.

decrease the cost.

### III. SPHERICAL ANTENNAS AND ANTENNA ARRAY

The spherical patch antenna would be a great candidate for conformal design and a near omni-directional radiation pattern along a plane. In this paper, an array of four patch antennas is realized are designed onto a sphere with 20 mm radius. The spherical patch antennas are 16.2 mm long to work at 5 GHz and 20 mm wide (bottom edge) to enable omni-directional coverage on the water level plane. The bottom edges of the spherical patch antennas are overlap with the mid-plane of the sphere to reduce the loss from water and adjust the radiation pattern.

In order to fully characterize the antenna, the two models shown in Fig. 3 are fabricated and measured with result demonstrated in Fig. 5&6 and Fig. 7&8, respectively. Fig. 5a shows both a great matching of the spherical patch antenna and more than 30 dB isolation with the antennas on the adjacent and the opposite sides. The higher resonant frequency in Fig. 5a and the higher gain in Fig. 5b featured by a ball partially submerged in the water are due to the high conductivity of the water that functions as an extended ground plane making the antenna more directive. This can be seen in the radiation patterns in Fig. 6a and Fig. 6b as well. To feed the four antennas with an equal phase, a 5-port power splitter

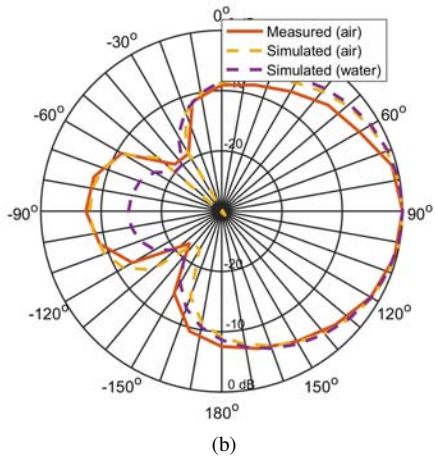
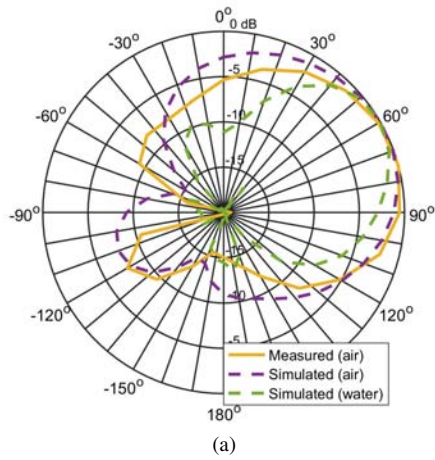


Fig. 6. Performance of the four individual antennas on the sphere. Measured and simulated values in air and simulated values in water for (a) normalized radiation pattern in  $\phi=90^\circ$  and (b) normalized radiation pattern in  $\theta=90^\circ$ .

is designed with 1.5 mm width for the quarter-wavelength impedance transformer and 0.7 mm width for the 100 Ohm microstrip line as shown in Fig. 3b. The array is well matched as shown in Fig. 7a and the measured gain agrees with the simulations as well in Fig. 7b. Fig. 8a shows a very good gain for  $\theta$  from  $45^\circ$  to  $75^\circ$ , which is effectively pointing above the water level and aiming to the shore/dam where the reader can be easily setup. Fig. 8b shows an omnidirectional gain over the  $\phi$  direction enabling reliable communication no matter how the ball rotates along  $\phi$ . This antenna provide a diversity in terms of space/direction which can be used in multiple-input and multiple-output (MIMO) applications.

#### IV. PHASE DELAY LINE SENSOR

A liquid-reconfigurable microstrip line topology including a signal line that is 3 mm long with a cross section of 1 mm  $\times$  1 mm and a distance of 1.6 mm from the horizontal ground plane (Fig. 9a) is designated as a reconfigurable phase delay line sensor. As shown in Fig. 9, the topology includes a liquid channel on top of the signal line with 0.5 mm distance and a ground plane on bottom. Typical water contamination liquids, especially organic ones such as oil (relative permittivity: 2.64), have a very low permittivity comparing to water (relative

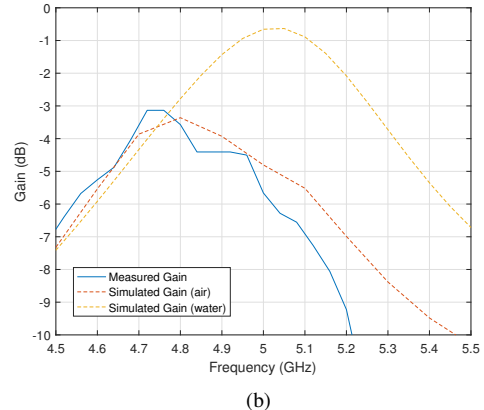
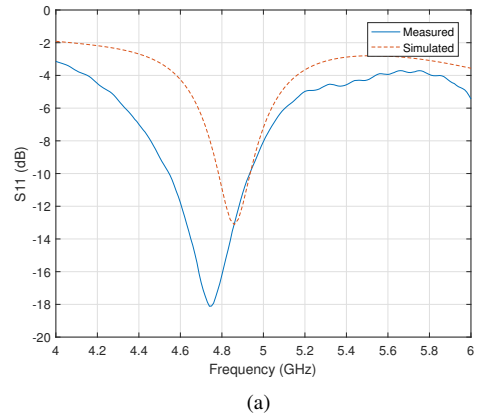


Fig. 7. Performance of the antenna array on the sphere. Measured and simulated values in air and simulated values in water for (a) return loss of the antenna and coupling between antennas and (b) gain.

permittivity: 78).[5] This dramatic change in the permittivity leads to a change of the effective permittivity of the microstrip line and thus additional phase introduced by that line. Fig. 9c shows the measured values of  $S_{11}$  of the phase delay line with the phase shift being almost linearly proportional to the relative permittivity values (e.g. 30 deg for an oil-filled channel). Therefore, by using this phase delay line to monitor the permittivity value of the liquid filling the channel, we can monitor if the water is contaminated by the oil or not.

#### V. CHIPLESS RFID

The spherical patch antenna on the top hemisphere and the phase delay line in the bottom hemisphere serve for communication and sensing purposes, respectively, effectively collecting and transmitting the contamination information in a chipless RFID fashion, as shown in Fig. 1. By adjusting the weight on the bottom of the ball, as shown in Fig. 1, the water level is designed to be right above the fluid channel and beneath the antenna feeding microstrip line as shown in Fig. 2b. In this way, the loss induced by water can be reduced and the contamination on water surface can be easily detected by the phase delay line sensor, that is folded towards the center of the ball so that the sensor is sensitive only to the liquid inside the channel without being sensitive to waves. Phase calibration can be performed effectively by utilizing the

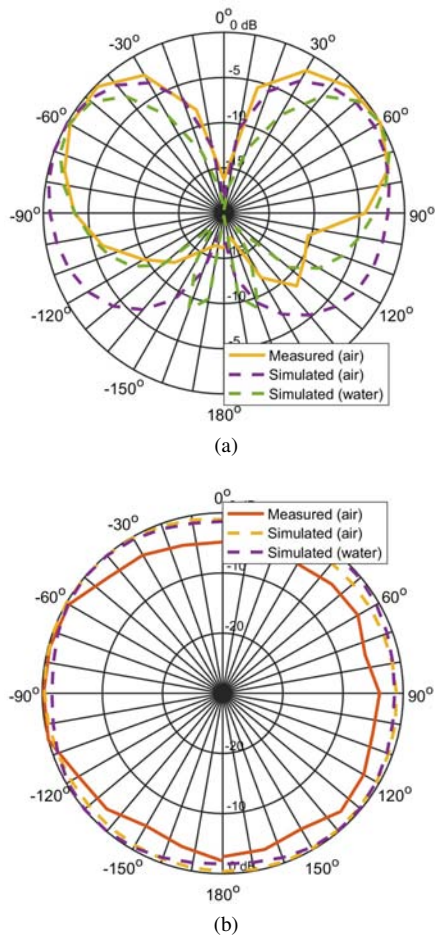


Fig. 8. Performance of the antenna array on the sphere. Measured and simulated values in air and simulated values in water for (a) normalized radiation pattern in  $\phi=90^\circ$  and (b) normalized radiation pattern in  $\theta=90^\circ$ .

phase of the reflection coefficient at the interface between the antenna feeding 50 Ohm line and the reconfigurable phase delay line as a reference phase.[6]. Fig. 10 shows an example circuit schematic of the equivalent chipless RFID configuration consisting of a reconfigurable phase delay microstrip line that is connected to the spherical patch antenna through a 2.7-mm wide and 5.7-mm long 50 Ohm microstrip line. The phase  $\Phi_0$  of the reflection from  $\Gamma_0$  between the two microstrip lines is not related to the liquid inside the channel while the phase  $\Phi_1$  of the reflection from  $\Gamma_1$  between the phase delay line and the open termination is changed with the permittivity of liquid inside of the channel. In this way, by dividing  $\Phi_0$  from  $\Phi_1$ , the phase difference induced by the phase delay line can be calculated.

## VI. CONCLUSION

This paper demonstrates a smart floating ball consisting spherical antennas and phase delay line sensors, which can be used in the water reservoir to detect the floating water contaminations such as oil and in other liquid monitoring such as crude leakage. The complex floating ball is fabricated by 3D printing dielectric balls without assembly and then selectively metalized by 3D printed conformal stamps, which provides a

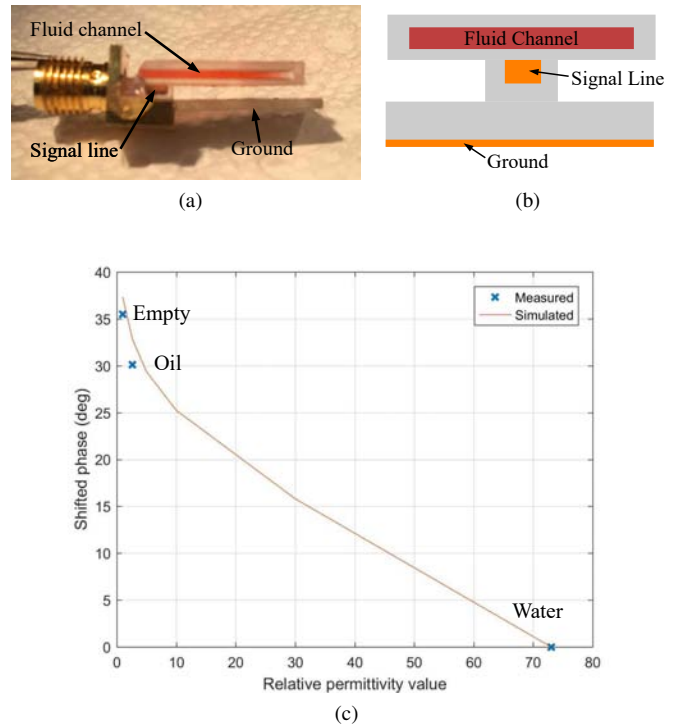


Fig. 9. (a) A photo of the phase delay line liquid sensor with red dyed water inside the 3D printed microfluidic channel. (b) A cross-section view of the phase delay microstrip line sensor. (c) Measured and simulated phase shift for different permittivity liquids inside the channel.

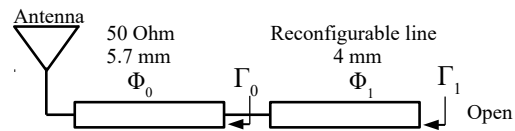


Fig. 10. Circuit schematic of the chipless RFID.

novel and straight-forward solution to selectively metalize 3D dielectric objects within same 3D printing platform.

## REFERENCES

- [1] W. Su, S. A. Nauroze, B. Ryan, and M. M. Tentzeris, "Novel 3d printed liquid-metal-alloy microfluidics-based zigzag and helical antennas for origami reconfigurable antenna trees," in *Microwave Symposium (IMS), 2017 IEEE MTT-S International*. IEEE, 2017, pp. 1579–1582.
- [2] R. A. Bahr, Y. Fang, W. Su, B. Tehrani, V. Palazzi, and M. M. Tentzeris, "Novel uniquely 3d printed intricate voronoi and fractal 3d antennas," in *Microwave Symposium (IMS), 2017 IEEE MTT-S International*. IEEE, 2017, pp. 1583–1586.
- [3] C. Garcia, R. Rumpf, H. Tsang, and J. Barton, "Effects of extreme surface roughness on 3d printed horn antenna," *Electronics Letters*, vol. 49, no. 12, pp. 734–736, 2013.
- [4] M. DAuria, W. J. Otter, J. Hazell, B. T. Gillatt, C. Long-Collins, N. M. Ridler, and S. Lucyszyn, "3-d printed metal-pipe rectangular waveguides," *IEEE Transactions on Components, Packaging and Manufacturing Technology*, vol. 5, no. 9, pp. 1339–1349, 2015.
- [5] V. Komarov, S. Wang, and J. Tang, "Permittivity and measurements," *Encyclopedia of RF and microwave engineering*, 2005.
- [6] M. Schüßler, C. Mandel, M. Maasch, A. Giere, and R. Jakoby, "Phase modulation scheme for chipless rfid-and wireless sensor tags," in *Microwave Conference, 2009. APMC 2009. Asia Pacific*. IEEE, 2009, pp. 229–232.